

000 001 002 003 004 005 LMGenDrive: LLM REASONING MEETS WORLD 006 MODELS FOR END-TO-END DRIVING 007 008 009

010 **Anonymous authors**
011 Paper under double-blind review
012
013
014
015
016
017
018
019
020
021
022
023
024
025
026
027
028
029
030
031
032
033
034
035
036

ABSTRACT

037 Recent years have witnessed remarkable progress in autonomous driving, yet generalization to long-tail and open-world scenarios remains the primary bottleneck
038 for large-scale deployment. To address this, one line of research explores LLMs
039 and VLMs for their vision-language understanding and reasoning capabilities,
040 equipping AVs with the ability not only to interpret rare and safety-critical situations
041 when generating driving actions. In parallel, another line investigates generative world
042 models to capture the spatio-temporal evolution of driving scenes, enabling agents to imagine and evaluate possible futures before acting. Inspired
043 by human intelligence, which seamlessly unites understanding and imagination
044 as a hallmark of AGI, this work explores a unified model that brings these two
045 capabilities together for autonomous driving. We present LMGenDrive, the first
046 framework that unifies LLM-based multimodal reasoning with generative world
047 models for end-to-end closed-loop autonomous driving. Given multi-view camera
048 inputs and natural-language instructions, our model generates both realistic
049 future driving videos and corresponding control signals. By coupling an LLM
050 with generative video capabilities, LMGenDrive gains complementary benefits:
051 future video prediction enhances the LLM’s spatio-temporal scene understanding,
052 while the LLM itself provides reasoning and instruction-following capabilities.
053 A progressive three-stage training strategy—ranging from vision pretraining to
054 multi-step long-horizon driving—is proposed to further improve stability and performance.
055 The resulting model can also operate in two complementary modes: low-latency online planning and autoregressive offline video generation. Experiments
056 show that LMGenDrive significantly outperforms state-of-the-art methods
057 on challenging closed-loop driving benchmarks, improving instruction following,
058 spatio-temporal reasoning, and robustness to rare scenarios. Our work not only
059 sets a new state-of-the-art in autonomous driving, but also demonstrates that unifying
060 multimodal understanding and generation offers a foundational new paradigm
061 toward achieving embodied AGI.
062
063

064 1 INTRODUCTION

065 Remarkable progress in autonomous driving has been witnessed in recent years with an increasing
066 number of commercial autonomous vehicles (AVs) deployed on public roads. Amidst this momentum,
067 end-to-end autonomous driving has emerged as a particularly vibrant research direction. Unlike
068 traditional modular pipelines that separately handle perception, prediction, and planning with hand-
069 crafted interfaces, end-to-end models provide a holistic paradigm with potential to remove information
070 bottlenecks among modules, better align model optimization with system-level performance,
071 and scale effectively with large amounts of driving data.

072 Despite this progress, the problem of generalization remains the central bottleneck for the entire
073 autonomous driving community. As we approach the frontier of real-world deployment, the ability
074 to robustly handle long-tail edge cases and operate in open-world settings remains the defining chal-
075 lenge for AV systems. These scenarios can include rare but safety-critical events, distribution shifts
076 across regions, adversarial weather conditions, as well as complex social interactions and ambigu-
077 ous intent among agents. This challenge manifests across the autonomy stack: perception systems
078 struggle to identify open-set entities, while prediction and planning models falter in extrapolating to

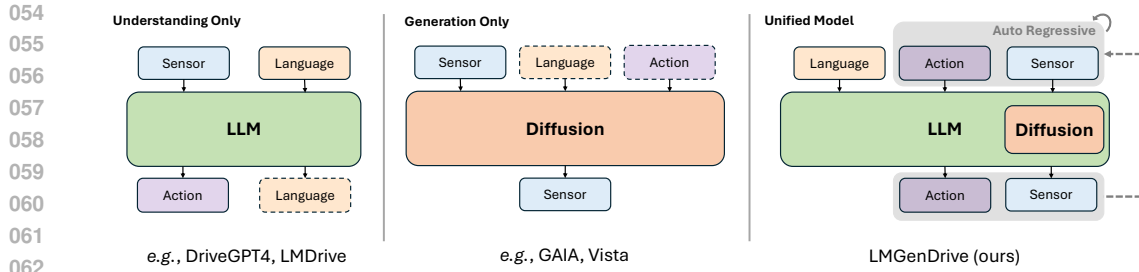


Figure 1: Comparison between existing works and ours. Prior works either leverage LLMs/VLMs for multimodal understanding and reasoning, or adopt world models for video-based scene imagination, but treat these capabilities in isolation. In contrast, our proposed **LMGenDrive** unifies both within a closed-loop end-to-end framework: the LLM interprets and reasons over multimodal inputs, while the world model simulates future scene evolution, together enabling instruction-guided planning, spatio-temporal reasoning, and robust long-horizon driving.

nondeterministic and previously unseen behaviors. These generalization failures represent the last barrier between research prototypes and truly scalable, globally deployable autonomous vehicles.

Amid this backdrop, large language models (LLMs) have emerged to demonstrate unprecedented reasoning and generalization abilities that approach—if not exceed—human-level performance. Recent models such as GPT-5 and DeepSeek-R1 (Guo et al., 2025) showcase robust capabilities in commonsense reasoning, abstraction, and decision-making. Meanwhile, vision-language models (VLMs) further extend this capacity to the multimodal domain, enabling unified interpretation of textual and visual inputs (Wang et al., 2025b; Bai et al., 2025; Liu et al., 2023; Li et al., 2022; Alayrac et al., 2022). Inspired by these vision-language understanding and reasoning capabilities, a wave of research has begun exploring how to equip AV systems with LLMs and VLMs to address the open-world, long-tail challenges in autonomous driving. As exemplified in works such as LMDrive (Shao et al., 2024) and GPT-Driver (Mao et al., 2023a), these models act as the cognitive brains to interpret ambiguous scenarios and guiding complex decision-making under uncertainty. However, most existing LLM- or VLM-empowered driving methods follow the paradigm that maps inputs directly to actions, falling short in explaining and capturing the temporal evolution of driving scenes—an essential factor for robust and anticipatory planning.

Meanwhile, another stream of research, world model (Ha & Schmidhuber, 2018), has emerged to simulate the spatio-temporal evolution of the scenes, as exemplified by video-based works such as Genie-3 (Ball et al., 2025) and Pandora (Xiang et al., 2024). Their potential has also been actively explored in the autonomous driving domain, enabling the agent to “imagine” different futures before committing to a plan. However, existing works either focus on solely generating high-fidelity scenes (Hu et al., 2023a; Russell et al., 2025; Gao et al., 2023; 2024; Ji et al., 2025; Wang et al., 2024a; Yang et al., 2024), or utilize world models as a plug-and-play forecasting module to rank multiple possible plans (Wang et al., 2024b; Wang & Peng, 2025). The integration of joint video generation and motion planning remains underexplored, limiting their ability to address critical challenges such as cumulative control errors, human-robot interaction, and the temporal consistency between generated actions and videos—factors that are essential for long-horizon problem solving in real-world systems. Moreover, these models generally lack the rich reasoning priors and instruction following capabilities uniquely offered by LLMs.

In contrast to existing models that specialize in either understanding or generation, human intelligence is inherently capable of both understanding the present and imagining the future—a dual capacity for perception and generation that underpins commonsense reasoning and long-horizon decision-making, suggesting a natural path toward artificial general intelligence (AGI). While recent studies (Deng et al., 2025; Shi et al., 2024; Chen et al., 2025; Liao et al., 2025) have shown encouraging results synergizing multimodal understanding and generation within a single model, whether this principle extends to embodied agents—and autonomous driving in particular—remains an open challenge. In this work, we propose LMGenDrive, the first framework that unifies LLM-based multimodal understanding with generative world models for closed-loop end-to-end autonomous driving. Our unified model takes multi-view camera data and natural-language driving instructions as inputs,

108 generating both multi-view future driving videos and control signals for the following timesteps.
 109 Concretely, we integrate an LLM and a diffusion-based video generation model: the LLM interprets
 110 and fuses visual observations with language instructions, producing learnable queries that capture
 111 the evolving scene states, which then serve as conditioning signals for the diffusion model to gener-
 112 ate realistic multi-view driving futures. Within this unified architecture, video generation enhances
 113 the LLM’s spatio-temporal scene understanding, while the LLM imparts instruction-following and
 114 reasoning capabilities to the world model—together yielding stronger and more robust closed-loop
 115 driving performance.

116 To enable such a unified model, we also propose a curriculum three-stage training strategy for en-
 117 hanced performance and stability. First, we pretrain a vision encoder for robust driving scene under-
 118 standing. Next, the frozen encoder is integrated with the LLM and video generator, and fine-tuned
 119 on single-step prediction to ground instruction following and immediate action outcomes. Finally,
 120 training is extended to multi-step sequences, enhancing long-horizon reasoning and temporal mod-
 121 eling for continuous driving scenarios. Once trained, the model can be applied in two modes: (1)
 122 Online planning mode: the model solely predicts planning outputs, with the diffusion generation
 123 component discarded to reduce latency; (2) Offline data generation mode: the model conducts au-
 124 toregressive video generation, where the generated video and predicted control signal serve as input
 125 for the next timestep, enabling extended and consistent driving video sequences.

126 To sum up, our contributions are threefold: (1) *Unified closed-loop framework*. We present LM-
 127 GenDrive, the first framework that unifies LLM-based multimodal understanding with generative
 128 world models for closed-loop end-to-end autonomous driving, bridging perception, reasoning, and
 129 imagination within a single architecture; (2) *Progressive training and dual modes*. We introduce
 130 a three-stage training pipeline—from vision pretraining in driving domain, to long-horizon multi-
 131 step driving—and support two usage modes: online planning for low-latency operation, and offline
 132 autoregressive video generation for extended sequences. (3) Through comprehensive experiments,
 133 LMGenDrive achieves state-of-the-art closed-loop performance on challenging autonomous driving
 134 benchmarks, improving instruction-following, spatio-temporal reasoning, and robustness to long-tail
 135 scenarios. Beyond performance gains, it provides experimental evidence that unifying multimodal
 136 understanding and generation yields complementary benefits, pointing toward a promising path for
 137 embodied AGI.

138 2 RELATED WORKS

140 2.1 END-TO-END DRIVING

142 Much progress has been made in end-to-end autonomous driving, with many recent methods based
 143 on imitation learning. UniAD (Hu et al., 2023b) unified full-stack driving tasks through query-based
 144 interfaces, while ThinkTwice (Jia et al., 2023b) retrieved critical-region information to refine pre-
 145 dictions. InterFuser (Shao et al., 2023a) used transformers to fuse multi-modal, multi-view sensor
 146 data for richer scene understanding. ReasonNet (Shao et al., 2023b) leveraged both temporal and
 147 global information of the driving scene to enhance perception, particularly in occlusion scenarios.
 148 Para-Drive (Weng et al., 2024) proposed a fully parallel architecture with a shared BEV representa-
 149 tion, and DriveTransformer (Jia et al., 2025) went further by discarding BEV features and using pure
 150 transformers to aggregate sensor and query information. Diffusion models have also emerged for
 151 modeling diverse driving behaviors. DiffusionPlanner (Zheng et al., 2025) applied a diffusion-based
 152 policy for flexible, personalized driving, and DiffAD (Wang et al., 2025a) formulated perception
 153 and decision-making as conditional image generation. Despite these advances, most approaches
 154 still struggle with rare corner cases and lack the reasoning ability needed to generalize beyond the
 155 training distribution.

156 2.2 MLLM FOR AUTONOMOUS DRIVING

158 Recent advances in large language models (LLMs) (Guo et al., 2025; Yang et al., 2025a; Touvron
 159 et al., 2023a;b; Jaeger et al., 2023a; Jia et al., 2023a) and vision–language models (VLMs) (Bai et al.,
 160 2025; Zhu et al., 2023; Liu et al., 2023; Wang et al., 2025b) have motivated integrating MLLMs into
 161 autonomous driving for stronger reasoning and explainability. Early works like GPT-Driver (Mao
 et al., 2023a) and LanguageMPC (Sha et al., 2023) convert driving scenes into textual inputs for

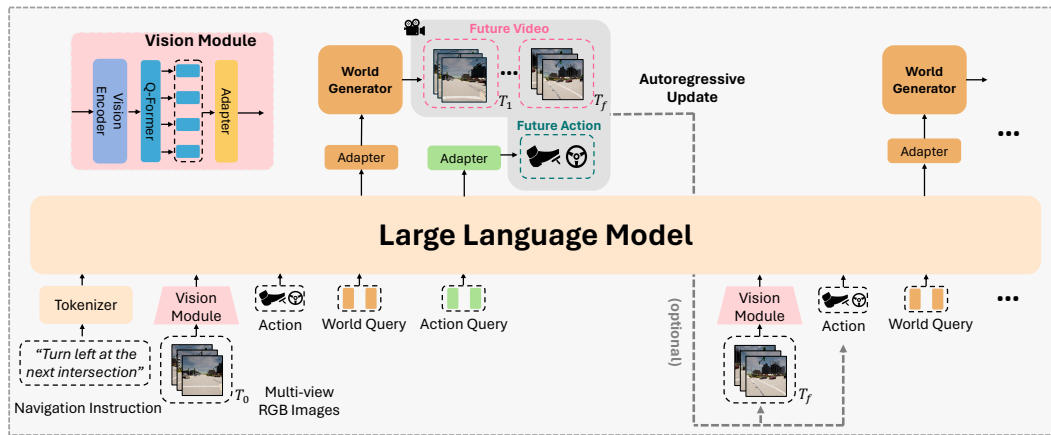


Figure 2: Overview of our unified understanding and generation architecture. We start by encoding the language instruction, multi-view RGB images, and the current action into the LLM. Two sets of learnable queries, world query and action query, are then fed into the LLM, and ultimately used to generate the future driving video and corresponding actions. The framework supports two operation modes: (1) offline data generation mode, an autoregressive generation process is adopted, where the last frame of the future video and the predicted action are used as inputs for the next timestep; (2) online planning mode, real-world data are provided as inputs for the following timestep.

direct reasoning. Later methods employ VLMs to process images and videos: some focus on visual question answering for scene understanding and optional action output (e.g., DriveLM (Sima et al., 2024), DriveGPT4 (Xu et al., 2023), DriveVLM (Tian et al., 2024)), while others predict driving actions end-to-end (e.g., LMDrive (Shao et al., 2024), DriveMoE (Yang et al., 2025b), BEV-Driver (Winter et al., 2025)). Agentic designs with hierarchical control, tool use, and memory, such as Agent-Driver (Mao et al., 2023b) and AD-H (Zhang et al., 2024), further extend capability. However, most MLLM-based approaches emphasize planning or explanation and lack robust modeling of how scenes and surrounding objects evolve over time—a key requirement for anticipating events and ensuring safe, long-horizon decision-making.

2.3 WORLD MODELS FOR AUTONOMOUS DRIVING

The concept of a *world model*, a predictive model that simulates environment dynamics, has regained attention. Video generation has become a leading paradigm, supported by advances in generative modeling, large-scale video datasets, and wide applicability. In autonomous driving, temporally grounded video prediction provides rich context for understanding and decision-making. Several methods treat pure video generation as world modeling. GAIA (Hu et al., 2023a) conditions generation on image, text, and action inputs. GAIA-2 (Russell et al., 2025) extends this to multi-view scenes, and MagicDrive (Gao et al., 2023) adds control signals such as HD maps and bounding boxes. Vista (Gao et al., 2024) scales to internet-scale driving data, while CoGen3D (Ji et al., 2025) predicts 3D-consistent representations before video synthesis to improve spatial coherence. Beyond pure generation, DriveWM (Wang et al., 2024b) predicts alternative futures for conditional planning. More recent work—DriveDreamer (Wang et al., 2024a), GenAD (Yang et al., 2024), and Prophet-DWM (Wang & Peng, 2025)—jointly models videos and actions but still mainly uses open-loop settings without direct feedback. The most related work is LAW (Li et al., 2024), which combines world modeling with closed-loop planning. However, it supervises the world model only with next-frame hidden features instead of full video generation, limiting its ability to simulate or create synthetic data. It also lacks language model integration and thus cannot handle instruction following, natural language grounding, or interactive human–AI communication in driving. To our knowledge, this is the first framework to unify LLM-based commonsense reasoning with video world models for closed-loop end-to-end autonomous driving.

216

3 METHOD

217

3.1 OVERALL FRAMEWORK

218 In this work, we propose LMGenDrive, a framework that unifies textual understanding/reasoning,
 219 future scene generation, and end-to-end planning. As illustrated in Figure 2, LMGenDrive is com-
 220 posed of three major components: (1) a vision encoder that processes multi-view camera sensor
 221 data for scene understanding and generating visual tokens; (2) a large language model and its asso-
 222 ciated component (tokenizer, Q-Former, and adapters) that takes in the language instruction, input
 223 visual tokens, world queries, and action queries, to predict the future driving scenes and actions;
 224 (3) a multi-view world generator that takes future scene tokens from the LLM and multi-view im-
 225 ages from the last frame as inputs, to generate future multi-view driving videos. We will introduce
 226 the vision encoder in Section 3.2, the LLM with its associated components in Section 3.3, and the
 227 multiview world generator in Section 3.4. Finally, we describe the training recipe in Section 3.5.
 228

229

3.2 VISION ENCODER

230 The vision encoder is designed to perceive the environment by processing, fusing, and transform-
 231 ing sensor data into visual tokens that can be consumed by the language model. Prior works (Shao
 232 et al., 2024; Jaeger et al., 2023b) typically leverage both multi-view images and LiDAR sensor in-
 233 puts, where the LiDAR inputs are encoded into bird’s-eye view (BEV) queries to extract information
 234 from multi-view images. However, our setting focuses on autoregressive video generation—where
 235 LiDAR is only available at the current frame but not in future frames. As a result, we replace Li-
 236 DAR inputs with BEV positional encodings, enabling effective perception while maintaining com-
 237 patibility with future video generation. The vision encoder consists of three parts: (1) In the sensor
 238 encoding part, for each image input, a 2D backbone Resnet (He et al., 2016) is applied to extract
 239 the image feature map, which is flattened to one-dimensional tokens. Tokens from different views
 240 are then fused by a transformer encoder. (2) In the BEV decoder, BEV position encodings serve as
 241 $H \times W$ queries to attend to the multi-view image features and generate BEV tokens. In addition, the
 242 learnable queries and one extra query generate corresponding waypoint tokens and one traffic-light
 243 token, respectively. The three types of visual tokens (BEV, waypoint, and traffic light) will be pre-
 244 sented to the LLM, providing rich scene information. (3) Lastly, as the first-stage training, the vision
 245 encoder is pretrained on perception tasks (BEV object detection, traffic light recognition, waypoint
 246 prediction) by feeding the three types of tokens to additional prediction heads. Three loss terms,
 247 including the detection loss (Shao et al., 2023b), the l_1 waypoint loss and the cross-entropy traffic
 248 light prediction loss, are applied respectively. Note that, following LMDrive (Shao et al., 2024),
 249 once pretrained, these prediction heads are discarded and the encoder is frozen, serving as the vision
 250 encoder for the large language model.
 251

252

3.3 LLM FOR INSTRUCTION-FOLLOWING DRIVING AND SCENE UNDERSTANDING

253 As depicted in Figure 2, our system casts the LLM as the “brain” of the entire driving pipeline: it in-
 254 gests sensor tokens emitted by the frozen vision encoder at every frame and parses natural-language
 255 commands, to forecast upcoming maneuvers and emits conditioning features for subsequent video
 256 generation. We adopt LLaMA (Touvron et al., 2023a) as the linguistic architecture due to its broad
 257 success in both language-centric (Zheng et al., 2023; Geng et al., 2023) and vision-grounded (Liu
 258 et al., 2023; Zhu et al., 2023) instruction-tuning settings.

259 **Instruction and visual tokenization.** As the model takes navigation instruction and multi-view
 260 image as inputs, their tokenization is our first step. For the navigation instruction, we tokenize
 261 them with the LLaMA tokenizer (Touvron et al., 2023a). For the multi-view images, each frame is
 262 tokenized by the aforementioned vision encoder, and the resulting tokens are buffered together with
 263 the most recent token history (up to T_{\max} frames) to curb cumulative error and maintain temporal
 264 coherence during executing the driving instruction in the closed loop. For each frame, the pretrained
 265 vision encoder outputs $H \times W$ BEV tokens, 4 waypoint tokens, and 1 traffic-light token. Passing all
 266 visual tokens (about 2k per frame) to the LLM is computationally prohibitive. To compress them, we
 267 use a Q-Former with 8 learnable queries per frame that attend to the raw tokens and distill them into
 268 compact frame-level features. An MLP adapter then projects these features to the LLM’s embedding
 269 dimension for seamless fusion with language tokens.

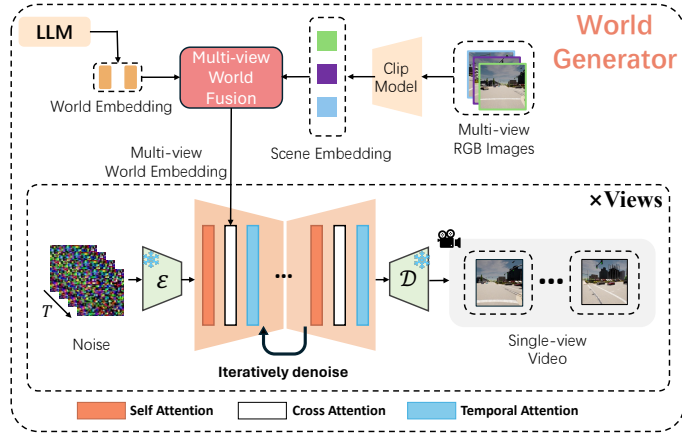


Figure 3: Architecture of our world generator. We begin by fusing the world embedding obtained from the LLM with multi-view RGB images. The fused multi-view world embedding is then injected into the diffusion model with the cross-attention mechanism to generate multi-view future videos.

Action prediction. Together with the instruction and visual tokens, we feed N learnable action query tokens into the LLM. After passing through the LLM and associated adapters, these queries evolve into N latent feature vectors, each encoding the spatio-temporal context needed for motion planning. A subsequent two-layer MLP maps these N feature vectors to N predicted waypoints and outputs a binary flag indicating whether the current instruction has been completed. Finally, the predicted waypoints are converted into low-level control commands—brake, throttle, and steering—through two independent PID controllers (Chen et al., 2020) that separately regulate longitudinal velocity and lateral heading, ensuring accurate trajectory tracking.

3.4 MULTI-VIEW WORLD MODEL

While the LLM is responsible for instruction following and reasoning, autonomous driving also requires modeling the visual dynamics of the environment. To this end, we introduce a multi-view world model that generates future video frames conditioned on the LLM outputs. By aligning action predictions with video generation, our framework jointly reasons about both the agent’s behavior and the evolution of the surrounding world. Our video generation process additionally *supports* an autoregressive mode (Xiang et al., 2024), which can be optionally enabled during inference: the future action and frame predicted at the previous timestep can be fed back into the LLM as input for the next prediction.

World Query Conditioning. As shown in Figure 2, in addition to the instructional tokens, visual tokens, and action query mentioned above, the LLM also takes the world query as input. Passing through the LLM, these world queries aggregate information from instructions, sensor inputs, and the actions, thereby enabling the model to form an internal representation of the world dynamics. Conceptually, these queries serve as a bridge to the world’s temporal evolution, and act as the conditioning signal fed into the following world generator to synthesize future driving videos.

Multi-view Image Conditioning. As shown in Figure 3, besides using scene queries to capture world evolution, we incorporate the last-frame multi-view images to supply fine-grained appearance details and the initial world state. These images are encoded by a CLIP model into semantically rich features that emphasize visual textures and appearance. During end-to-end training, these CLIP features are fused with LLM representations through attention blocks. Self-attention aggregates and aligns multi-view information into a unified space, and cross-attention injects LLM guidance. This design not only provides an appearance prior for consistent video generation but also encourages the LLM to focus on dynamic, motion-related representations.

World Generator. After the multi-view world fusion step, we obtain a set of multi-view world embeddings, each corresponding to one camera view. Taking these embeddings as the final conditioning feature, our world generator employs a U-Net (Ronneberger et al., 2015) diffusion architecture

324 to produce future frames. For each view, the associated embedding is injected into the diffusion
 325 process through a dedicated cross-attention module, ensuring that view-specific information is ef-
 326 fectively transferred. The model follows the standard denoising diffusion process (Ho et al., 2020):
 327 starting from pure Gaussian noise and progressively removing noise to generate a future video se-
 328 quence. The output is a video tensor of shape $\mathbb{R}^{v \times t \times h \times w \times 3}$, where v is the number of views, t is
 329 the temporal length, and h, w are the spatial resolution. Inspired by (Wang et al., 2024b; Guo et al.,
 330 2023), we further augment the U-Net blocks with spatio-temporal transformers to better capture
 331 temporal dynamics and spatial structure in driving scenes.

332 3.5 TRAINING RECIPE

333 We adopt a three-stage training strategy to progressively build the model’s perception, reasoning,
 334 and generation capabilities. This curriculum ensures stable convergence and enables effective long-
 335 horizon temporal modeling.

336 **Stage 1: Vision Encoder Pretraining.** We first pretrain the vision encoder on single-frame percep-
 337 tion tasks using 3M expert-collected frames from CARLA (Shao et al., 2023a). Perception heads are
 338 attached for object detection, traffic light classification, and waypoint regression. After convergence,
 339 only the vision encoder is retained and frozen in later stages.

340 **Stage 2: Single-Step Planning and Generation.** Next, we jointly fine-tune the LLM and the video
 341 generator for single-step prediction. The vision encoder is frozen to reduce memory usage. The
 342 model takes as input a single-frame multi-view image, natural language instruction, action queries,
 343 and world queries, to predict the next waypoint, the instruction completion flag, and the future
 344 driving video. This stage enables the LLM to learn grounded instruction-following and understand
 345 how the world evolves under given actions. Simultaneously, the world generator learns to synthesize
 346 multi-view driving videos conditioned on the last frame and LLM-generated features.

347 **Stage 3: Multi-Step Long-Horizon Training.** We progressively expand training to 2–3-step se-
 348 quences to strengthen long-horizon reasoning. Specifically, previously generated videos are au-
 349 toregressively fed as input for the next step’s generation. To save memory, the video generator
 350 is frozen while gradients still propagate, and the LLM remains fully trainable. This design en-
 351 courages the LLM to capture temporal dependencies—such as other agents’ intentions, speed, and
 352 interactions—over extended observation windows. As a result, the LLM develops stronger temporal
 353 abstraction and inductive reasoning abilities for dynamic driving scenes.

354 **Training Objectives.** We apply three loss terms in the last two stages: (1) l_1 waypoint regression
 355 loss; (2) binary classification loss for instruction completion; (3) diffusion loss for video generation:

$$\mathcal{L}_{\text{DM}} = \mathbb{E}_{t, \epsilon} \left[\|\epsilon_\theta(\mathbf{z}_t, \mathbf{c}, t) - \epsilon\|^2 \right],$$

356 where \mathbf{z}_t is the noisy latent at timestep t , ϵ is the added Gaussian noise, and \mathbf{c} denotes conditioning
 357 features from the multi-view image and scene queries.

363 4 EXPERIMENTS

364 4.1 EXPERIMENT SETUP

365 **Training Details.** During training, three synchronized RGB cameras (left, front, right) are resized
 366 to 224^2 pixels and sampled at 10 Hz, and an 8-frame temporal window is considered. The network
 367 is tasked with predicting four future waypoints at $t + \{0.2, 0.4, 0.6, 0.8\}$ s, along with eight future
 368 video frames from $t + 0.1$ s to $t + 0.9$ s in 0.1-second increments. We optimize the model using
 369 AdamW optimizer (Loshchilov & Hutter, 2018) with an initial learning rate of 1×10^{-5} on eight
 370 NVIDIA H800 GPUs under DeepSpeed ZeRO-2; convergence is reached in roughly two days. Due
 371 to GPU-memory constraints, the third training stage operates on one to three timesteps. The system
 372 uses Vicuna-7B (Chiang et al., 2023) as the LLM backbone, Stable Diffusion 1.5 (Rombach et al.,
 373 2022) for image generation, and AnimateDiff (Guo et al., 2023) for temporal modeling.

374 **Benchmark.** We implement and evaluate our approach using the open-source CARLA simulator
 375 of version 0.9.10.1 (Dosovitskiy et al., 2017) on the LangAuto benchmark (Shao et al., 2024). The
 376 LangAuto benchmark comprises test routes that traverse eight CARLA towns, span diverse weather

378 settings, and contain deliberately misleading linguistic cues. It consists of three tracks, LangAuto,
 379 LangAuto-Short, and LangAuto-Tiny, which varies in the route length. During evaluation, each
 380 method controls the vehicle using only natural-language commands and visual observations.
 381

382 **Metric.** Following the CARLA Leaderboard (CARLA Team, 2020) and LangAuto (Shao et al.,
 383 2024), we report route completion (RC), infraction score (IS), and driving score (DS). RC measures
 384 the fraction of the planned route completed before exceeding the deviation tolerance. IS penalizes
 385 collisions and traffic-rule violations via a decaying factor. DS, the product of RC and IS, serves as
 386 the primary overall indicator of safe and efficient driving. For generated videos, we further evaluate
 387 perceptual quality using Fréchet Video Distance (FVD) and Fréchet Inception Distance (FID), which
 388 assess temporal consistency and visual realism, respectively.

389 4.2 SOTA COMPARISON

391 Methods	392 LangAuto			393 LangAuto-Short			394 LangAuto-Tiny		
	395 DS \uparrow	396 RC \uparrow	397 IS \uparrow	398 DS \uparrow	399 RC \uparrow	400 IS \uparrow	401 DS \uparrow	402 RC \uparrow	403 IS \uparrow
LMDrive (Shao et al., 2024)	10.7 \pm 3.8	16.2 \pm 4.9	0.63 \pm 0.04	14.2 \pm 4.4	20.1 \pm 4.4	0.72 \pm 0.04	20.1 \pm 4.1	24.7 \pm 5.1	0.75 \pm 0.03
AD-H \dagger (Zhang et al., 2024)	44.0	53.2	0.83	56.1	68.0	0.78	77.5	85.1	0.91
BEVDriver (Winter et al., 2025)	48.9	59.7	0.82	66.7	77.8	0.87	70.2	81.3	0.87
Ours	62.2\pm3.3	74.5\pm4.1	0.85\pm0.04	77.1\pm4.1	87.9\pm3.5	0.88\pm0.03	84.1\pm3.6	92.5\pm4.0	0.92\pm0.04

396 Table 1: Performance comparison on the LangAuto benchmark. We report the metrics for 3 evalua-
 397 tion runs. AD-H \dagger leverages an extra model OPT-350M (Zhang et al., 2022) for low-level control.
 398

399 The experimental results in Table 1 demonstrate that our method significantly outperforms existing
 400 state-of-the-art approaches on the LangAuto benchmark. Specifically, LMDrive (Shao et al., 2024)
 401 achieves a driving score (DS) of 10.7 in the LangAuto track, while AD-H (Zhang et al., 2024) and
 402 BEVDriver (Winter et al., 2025) demonstrates improved DS values of 44.0 and 48.9, respectively.
 403 Our method further push the performance to a higher level, with a DS of 62.2. In terms of route
 404 completion (RC) and infraction score (IS), our approach also shows superior performance across
 405 all three tracks: LangAuto, LangAuto-Short, and LangAuto-Tiny, showing the effectiveness of our
 406 method in handling more complex driving scenarios with language instructions.

407 4.3 ABLATION STUDIES

409 Module design	410 DS \uparrow	411 RC \uparrow	412 IS \uparrow	413 Module design	414 FID \downarrow	415 FVD \downarrow
	416 baseline	417 62.2\pm3.3	418 74.5\pm4.1	419 0.85\pm0.04	420 baseline	421 6.3
w/o world generator	53.4 \pm 2.2	65.8 \pm 4.2	0.80 \pm 0.01	w/o multi-view fusion	7.8	371
w/o action queries	58.7 \pm 3.1	70.4 \pm 3.7	0.84 \pm 0.02	world queries: 64 \rightarrow 32	10.1	318
w/o visual pre-training	54.9 \pm 4.5	67.1 \pm 4.5	0.81 \pm 0.02	world queries: 64 \rightarrow 16	11.6	424
w/o stage-3 training	55.6 \pm 4.5	68.9 \pm 4.5	0.80 \pm 0.02			

416 Table 2: Ablation study on the module design for planning
 417 performance.

418 **Ablation Study on Module Design.** As shown in Table 2, we conduct four ablation experiments to
 419 quantify the contribution of each key component in our proposed LMGenDrive. (1) **w/o world gen-
 420 erator:** Removing the world generator together with its world query sharply degrades DS to 53.4,
 421 demonstrating that the multi-view world generator is crucial for enriching the LLM’s understanding
 422 of spatio-temporal dynamics and strengthening future-scene reasoning. (2) **w/o action queries:** Re-
 423 placing learnable action queries with an LMDrive-style autoregressive action prediction lowers DS
 424 to 58.7, indicating that explicit action queries provide more structured supervision and lead to more
 425 reliable planning. (3) **w/o visual pre-training:** Without the first-stage driving-oriented visual pre-
 426 training, DS drops to 54.9, highlighting the importance of injecting driving-specific semantics into
 427 the vision encoder to enhance downstream scene understanding. (4) **w/o stage-3 training:** Skip-
 428 ping the Multi-Step Long-Horizon training stage reduces DS to 55.6, confirming that long-horizon
 429 temporal modeling is essential for robust reasoning over extended driving contexts. Overall, all abla-
 430 tions shows degraded DS, with missing world generator or long-horizon training causing the largest
 431 drops, confirming these modules—along with visual pre-training and action queries—are vital for
 accurate, safe planning in LMGenDrive.

416 Table 3: Ablation study on the module
 417 design for generation performance.

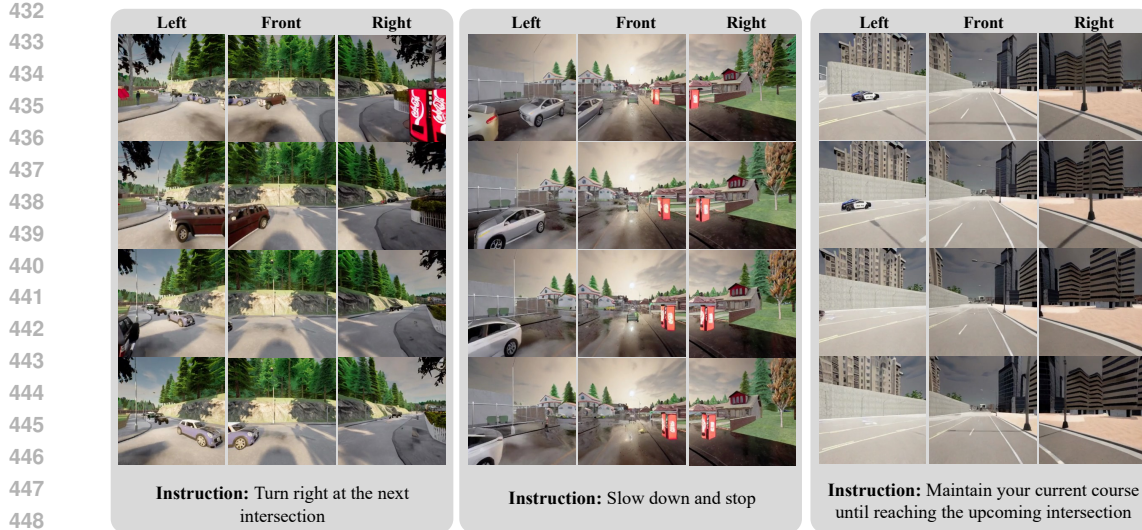


Figure 4: Visualization of multi-view future scenes generated by LMGenDrive, showing consistent left-front-right views aligned with driving instructions.

Ablation Study on Generation Module Design. As shown in Table 3, we further investigate how key components of the generation module influence video quality, measured by FID and FVD. (1) **w/o multi-view fusion**: Removing the cross-view fusion increases FID from 6.3 to 7.8 and FVD from 286 to 371, indicating that, without interaction among different camera views, the model struggles to maintain spatial consistency. (2) **world queries choices**: Reducing the number of world queries from 64 to 32 or 16 leads to a clear performance drop, with FID/FVD rising to 10.1/318 and 11.6/424, respectively. Overall, these results demonstrate that multi-view fusion and sufficient world queries are critical for generating coherent, high-quality videos.

4.4 VISUALIZATION

To illustrate LMGenDrive’s capabilities, Figure 4 presents qualitative rollouts from the CARLA simulator. The top row shows the initial multi-view observations as the conditioning inputs, while the subsequent rows visualize three future steps generated by our multi-view world model in an autoregressive manner. At each step, the model takes the previously generated multi-view frames and predicts actions as input, to synthesize the next set of left, front, and right camera views. Each panel displays these synchronized camera views together with the corresponding driving instruction. The results show that LMGenDrive (1) preserves spatial consistency across views, (2) anticipates dynamic agents such as crossing vehicles and pedestrians, and (3) aligns future scene evolution with the given language instructions.

5 CONCLUSION

We introduced LMGenDrive, a unified framework that couples LLM-based multimodal understanding/reasoning with generative world models for closed-loop end-to-end autonomous driving. Through synergistic integration of instruction following, spatio-temporal reasoning, and realistic video generation, LMGenDrive significantly outperforms state-of-the-art methods on the CARLA LangAuto benchmark. Ablation studies verify the necessity of each core module, and results underscore the complementary benefits of unifying understanding and generation. This work offers a solid step toward embodied AGI and provides a foundation for future exploration on real-world deployment and broader cross-domain generalization.

486 REFERENCES
487

488 Jean-Baptiste Alayrac, Jeff Donahue, Pauline Luc, Antoine Miech, Iain Barr, Yana Hasson, Karel
489 Lenc, Arthur Mensch, Katherine Millican, Malcolm Reynolds, et al. Flamingo: a visual language
490 model for few-shot learning. *Advances in neural information processing systems*, 35:23716–
491 23736, 2022.

492 Shuai Bai, Keqin Chen, Xuejing Liu, Jialin Wang, Wenbin Ge, Sibo Song, Kai Dang, Peng Wang,
493 Shijie Wang, Jun Tang, et al. Qwen2. 5-vl technical report. *arXiv preprint arXiv:2502.13923*,
494 2025.

495 Philip J Ball, J Bauer, F Belletti, et al. Genie 3: A new frontier for world models, 2025.

496 CARLA Team. Carla autonomous driving leaderboard. <https://leaderboard.carla.org/>, 2020. Accessed: 2021-02-11.

497 Dian Chen, Brady Zhou, Vladlen Koltun, and Philipp Krähenbühl. Learning by cheating. In *Con-
498 ference on Robot Learning*, pp. 66–75. PMLR, 2020.

499 Jiupei Chen, Zhiyang Xu, Xichen Pan, Yushi Hu, Can Qin, Tom Goldstein, Lifu Huang, Tianyi
500 Zhou, Saining Xie, Silvio Savarese, et al. Blip3-o: A family of fully open unified multimodal
501 models-architecture, training and dataset. *arXiv preprint arXiv:2505.09568*, 2025.

502 Wei-Lin Chiang, Zhuohan Li, Ziqing Lin, Ying Sheng, Zhanghao Wu, Hao Zhang, Lianmin Zheng,
503 Siyuan Zhuang, Yonghao Zhuang, Joseph E Gonzalez, et al. Vicuna: An open-source chatbot
504 impressing gpt-4 with 90%* chatgpt quality. See <https://vicuna.lmsys.org> (accessed 14 April
505 2023), 2(3):6, 2023.

506 Chaorui Deng, Deyao Zhu, Kunchang Li, Chenhui Gou, Feng Li, Zeyu Wang, Shu Zhong, Weihao
507 Yu, Xiaonan Nie, Ziang Song, et al. Emerging properties in unified multimodal pretraining. *arXiv
508 preprint arXiv:2505.14683*, 2025.

509 Alexey Dosovitskiy, German Ros, Felipe Codevilla, Antonio Lopez, and Vladlen Koltun. Carla: An
510 open urban driving simulator. In *Conference on robot learning*, pp. 1–16. PMLR, 2017.

511 Ruiyuan Gao, Kai Chen, Enze Xie, Lanqing Hong, Zhenguo Li, Dit-Yan Yeung, and Qiang
512 Xu. Magicdrive: Street view generation with diverse 3d geometry control. *arXiv preprint
513 arXiv:2310.02601*, 2023.

514 Shenyuan Gao, Jiazheng Yang, Li Chen, Kashyap Chitta, Yihang Qiu, Andreas Geiger, Jun Zhang,
515 and Hongyang Li. Vista: A generalizable driving world model with high fidelity and versatile
516 controllability. *arXiv preprint arXiv:2405.17398*, 2024.

517 Xinyang Geng, Arnav Gudibande, Hao Liu, Eric Wallace, Pieter Abbeel, Sergey Levine, and Dawn
518 Song. Koala: A dialogue model for academic research. *Blog post*, April, 1, 2023.

519 Daya Guo, Dejian Yang, Haowei Zhang, Junxiao Song, Ruoyu Zhang, Runxin Xu, Qihao Zhu,
520 Shirong Ma, Peiyi Wang, Xiao Bi, et al. Deepseek-r1: Incentivizing reasoning capability in llms
521 via reinforcement learning. *arXiv preprint arXiv:2501.12948*, 2025.

522 Yuwei Guo, Ceyuan Yang, Anyi Rao, Zhengyang Liang, Yaohui Wang, Yu Qiao, Maneesh
523 Agrawala, Dahua Lin, and Bo Dai. Animatediff: Animate your personalized text-to-image diffu-
524 sion models without specific tuning. *arXiv preprint arXiv:2307.04725*, 2023.

525 David Ha and Jürgen Schmidhuber. World models. *arXiv preprint arXiv:1803.10122*, 2018.

526 Kaiming He, Xiangyu Zhang, Shaoqing Ren, and Jian Sun. Deep residual learning for image recog-
527 nition. In *Proceedings of the IEEE conference on computer vision and pattern recognition*, pp.
528 770–778, 2016.

529 Jonathan Ho, Ajay Jain, and Pieter Abbeel. Denoising diffusion probabilistic models. *Advances in
530 neural information processing systems*, 33:6840–6851, 2020.

540 Anthony Hu, Lloyd Russell, Hudson Yeo, Zak Murez, George Fedoseev, Alex Kendall, Jamie Shot-
 541 ton, and Gianluca Corrado. Gaia-1: A generative world model for autonomous driving. *arXiv*
 542 *preprint arXiv:2309.17080*, 2023a.

543 Yihan Hu, Jiazhi Yang, Li Chen, Keyu Li, Chonghao Sima, Xizhou Zhu, Siqi Chai, Senyao Du,
 544 Tianwei Lin, Wenhui Wang, et al. Planning-oriented autonomous driving. In *Proceedings of the*
 545 *IEEE/CVF Conference on Computer Vision and Pattern Recognition*, pp. 17853–17862, 2023b.

546 Bernhard Jaeger, Kashyap Chitta, and Andreas Geiger. Hidden biases of end-to-end driving models.
 547 2023a.

548 Bernhard Jaeger, Kashyap Chitta, and Andreas Geiger. Hidden biases of end-to-end driving models.
 549 *arXiv preprint arXiv:2306.07957*, 2023b.

550 Yishen Ji, Ziyue Zhu, Zhenxin Zhu, Kaixin Xiong, Ming Lu, Zhiqi Li, Lijun Zhou, Haiyang Sun,
 551 Bing Wang, and Tong Lu. Cogen: 3d consistent video generation via adaptive conditioning for
 552 autonomous driving. *arXiv preprint arXiv:2503.22231*, 2025.

553 Xiaosong Jia, Yulu Gao, Li Chen, Junchi Yan, Patrick Langechuan Liu, and Hongyang Li.
 554 Driveadapter: Breaking the coupling barrier of perception and planning in end-to-end autonomous
 555 driving. In *Proceedings of the IEEE/CVF International Conference on Computer Vision*, pp.
 556 7953–7963, 2023a.

557 Xiaosong Jia, Penghao Wu, Li Chen, Jiangwei Xie, Conghui He, Junchi Yan, and Hongyang Li.
 558 Think twice before driving: Towards scalable decoders for end-to-end autonomous driving. In
 559 *Proceedings of the IEEE/CVF Conference on Computer Vision and Pattern Recognition*, pp.
 560 21983–21994, 2023b.

561 Xiaosong Jia, Junqi You, Zhiyuan Zhang, and Junchi Yan. Drivetransformer: Unified transformer
 562 for scalable end-to-end autonomous driving. *arXiv preprint arXiv:2503.07656*, 2025.

563 Junnan Li, Dongxu Li, Caiming Xiong, and Steven Hoi. Blip: Bootstrapping language-image pre-
 564 training for unified vision-language understanding and generation. In *International conference on*
 565 *machine learning*, pp. 12888–12900. PMLR, 2022.

566 Yingyan Li, Lue Fan, Jiawei He, Yuqi Wang, Yuntao Chen, Zhaoxiang Zhang, and Tieniu
 567 Tan. Enhancing end-to-end autonomous driving with latent world model. *arXiv preprint*
 568 *arXiv:2406.08481*, 2024.

569 Chao Liao, Liyang Liu, Xun Wang, Zhengxiong Luo, Xinyu Zhang, Wenliang Zhao, Jie Wu, Liang
 570 Li, Zhi Tian, and Weilin Huang. Mogao: An omni foundation model for interleaved multi-modal
 571 generation. *arXiv preprint arXiv:2505.05472*, 2025.

572 Haotian Liu, Chunyuan Li, Qingyang Wu, and Yong Jae Lee. Visual instruction tuning. *Advances*
 573 *in neural information processing systems*, 36:34892–34916, 2023.

574 Ilya Loshchilov and Frank Hutter. Decoupled weight decay regularization. In *International Confer-
 575 ence on Learning Representations*, 2018.

576 Jiageng Mao, Yuxi Qian, Junjie Ye, Hang Zhao, and Yue Wang. Gpt-driver: Learning to drive with
 577 gpt. *arXiv preprint arXiv:2310.01415*, 2023a.

578 Jiageng Mao, Junjie Ye, Yuxi Qian, Marco Pavone, and Yue Wang. A language agent for autonomous
 579 driving. *arXiv preprint arXiv:2311.10813*, 2023b.

580 Robin Rombach, Andreas Blattmann, Dominik Lorenz, Patrick Esser, and Björn Ommer. High-
 581 resolution image synthesis with latent diffusion models. In *Proceedings of the IEEE/CVF confer-
 582 ence on computer vision and pattern recognition*, pp. 10684–10695, 2022.

583 Olaf Ronneberger, Philipp Fischer, and Thomas Brox. U-net: Convolutional networks for biomedical
 584 image segmentation. In *Medical image computing and computer-assisted intervention-MICCAI 2015: 18th international conference, Munich, Germany, October 5-9, 2015, proceed-
 585 ings, part III 18*, pp. 234–241. Springer, 2015.

594 Lloyd Russell, Anthony Hu, Lorenzo Bertoni, George Fedoseev, Jamie Shotton, Elahe Arani, and
 595 Gianluca Corrado. Gaia-2: A controllable multi-view generative world model for autonomous
 596 driving. *arXiv preprint arXiv:2503.20523*, 2025.

597

598 Hao Sha, Yao Mu, Yuxuan Jiang, Li Chen, Chenfeng Xu, Ping Luo, Shengbo Eben Li, Masayoshi
 599 Tomizuka, Wei Zhan, and Mingyu Ding. Languagempc: Large language models as decision
 600 makers for autonomous driving. *arXiv preprint arXiv:2310.03026*, 2023.

601 Hao Shao, Letian Wang, Ruobing Chen, Hongsheng Li, and Yu Liu. Safety-enhanced autonomous
 602 driving using interpretable sensor fusion transformer. In *Conference on Robot Learning*, pp. 726–
 603 737. PMLR, 2023a.

604 Hao Shao, Letian Wang, Ruobing Chen, Steven L Waslander, Hongsheng Li, and Yu Liu. Reason-
 605 net: End-to-end driving with temporal and global reasoning. In *Proceedings of the IEEE/CVF*
 606 *Conference on Computer Vision and Pattern Recognition*, pp. 13723–13733, 2023b.

607

608 Hao Shao, Yuxuan Hu, Letian Wang, Guanglu Song, Steven L Waslander, Yu Liu, and Hongsheng
 609 Li. Lmdrive: Closed-loop end-to-end driving with large language models. In *Proceedings of the*
 610 *IEEE/CVF Conference on Computer Vision and Pattern Recognition*, pp. 15120–15130, 2024.

611 Weijia Shi, Xiaochuang Han, Chunting Zhou, Weixin Liang, Xi Victoria Lin, Luke Zettlemoyer,
 612 and Lili Yu. Lmfusion: Adapting pretrained language models for multimodal generation. *arXiv*
 613 *preprint arXiv:2412.15188*, 2024.

614

615 Chonghao Sima, Katrin Renz, Kashyap Chitta, Li Chen, Hanxue Zhang, Chengen Xie, Jens
 616 Beißwenger, Ping Luo, Andreas Geiger, and Hongyang Li. Drivelm: Driving with graph vi-
 617 sual question answering. In *European Conference on Computer Vision*, pp. 256–274. Springer,
 618 2024.

619 Xiaoyu Tian, Junru Gu, Bailin Li, Yicheng Liu, Yang Wang, Zhiyong Zhao, Kun Zhan, Peng Jia,
 620 Xianpeng Lang, and Hang Zhao. Drivevilm: The convergence of autonomous driving and large
 621 vision-language models. *arXiv preprint arXiv:2402.12289*, 2024.

622

623 Hugo Touvron, Thibaut Lavril, Gautier Izacard, Xavier Martinet, Marie-Anne Lachaux, Timothée
 624 Lacroix, Baptiste Rozière, Naman Goyal, Eric Hambro, Faisal Azhar, et al. Llama: Open and
 625 efficient foundation language models. *arXiv preprint arXiv:2302.13971*, 2023a.

626 Hugo Touvron, Louis Martin, Kevin Stone, Peter Albert, Amjad Almahairi, Yasmine Babaei, Niko-
 627 lay Bashlykov, Soumya Batra, Prajjwal Bhargava, Shruti Bhosale, et al. Llama 2: Open founda-
 628 tion and fine-tuned chat models. *arXiv preprint arXiv:2307.09288*, 2023b.

629

630 Tao Wang, Cong Zhang, Xingguang Qu, Kun Li, Weiwei Liu, and Chang Huang. Diffad: A unified
 631 diffusion modeling approach for autonomous driving. *arXiv preprint arXiv:2503.12170*, 2025a.

632

633 Weiyun Wang, Zhangwei Gao, Lixin Gu, Hengjun Pu, Long Cui, Xingguang Wei, Zhaoyang Liu,
 634 Linglin Jing, Shenglong Ye, Jie Shao, et al. Internvl3. 5: Advancing open-source multimodal
 635 models in versatility, reasoning, and efficiency. *arXiv preprint arXiv:2508.18265*, 2025b.

636

637 Xiaodong Wang and Peixi Peng. Prophetdwm: A driving world model for rolling out future actions
 638 and videos. *arXiv preprint arXiv:2505.18650*, 2025.

639

640 Xiaofeng Wang, Zheng Zhu, Guan Huang, Xinze Chen, Jiagang Zhu, and Jiwen Lu. Drivedreamer:
 641 Towards real-world-drive world models for autonomous driving. In *European Conference on*
 642 *Computer Vision*, pp. 55–72. Springer, 2024a.

643

644 Yuqi Wang, Jiawei He, Lue Fan, Hongxin Li, Yuntao Chen, and Zhaoxiang Zhang. Driving into
 645 the future: Multiview visual forecasting and planning with world model for autonomous driving.
 646 In *Proceedings of the IEEE/CVF Conference on Computer Vision and Pattern Recognition*, pp.
 647 14749–14759, 2024b.

648

649 Xinshuo Weng, Boris Ivanovic, Yan Wang, Yue Wang, and Marco Pavone. Para-drive: Parallelized
 650 architecture for real-time autonomous driving. In *Proceedings of the IEEE/CVF Conference on*
 651 *Computer Vision and Pattern Recognition*, pp. 15449–15458, 2024.

648 Katharina Winter, Mark Azer, and Fabian B Flohr. Bevdriver: Leveraging bev maps in llms for
 649 robust closed-loop driving. *arXiv preprint arXiv:2503.03074*, 2025.
 650

651 Jiannan Xiang, Guangyi Liu, Yi Gu, Qiyue Gao, Yuting Ning, Yuheng Zha, Zeyu Feng, Tianhua
 652 Tao, Shibo Hao, Yemin Shi, et al. Pandora: Towards general world model with natural language
 653 actions and video states. *arXiv preprint arXiv:2406.09455*, 2024.

654 Zhenhua Xu, Yujia Zhang, Enze Xie, Zhen Zhao, Yong Guo, Kenneth KY Wong, Zhenguo Li, and
 655 Hengshuang Zhao. Drivegpt4: Interpretable end-to-end autonomous driving via large language
 656 model. *arXiv preprint arXiv:2310.01412*, 2023.
 657

658 An Yang, Anfeng Li, Baosong Yang, Beichen Zhang, Binyuan Hui, Bo Zheng, Bowen Yu,
 659 Chang Gao, Chengan Huang, Chenxu Lv, et al. Qwen3 technical report. *arXiv preprint
 660 arXiv:2505.09388*, 2025a.

661 Jiazhi Yang, Shenyuan Gao, Yihang Qiu, Li Chen, Tianyu Li, Bo Dai, Kashyap Chitta, Penghao Wu,
 662 Jia Zeng, Ping Luo, et al. Generalized predictive model for autonomous driving. In *Proceedings
 663 of the IEEE/CVF Conference on Computer Vision and Pattern Recognition*, pp. 14662–14672,
 664 2024.

665 Zhenjie Yang, Yilin Chai, Xiaosong Jia, Qifeng Li, Yuqian Shao, Xuekai Zhu, Haisheng Su, and
 666 Junchi Yan. Drivemoe: Mixture-of-experts for vision-language-action model in end-to-end au-
 667 tonomous driving. *arXiv preprint arXiv:2505.16278*, 2025b.
 668

669 Susan Zhang, Stephen Roller, Naman Goyal, Mikel Artetxe, Moya Chen, Shuohui Chen, Christo-
 670 pher Dewan, Mona Diab, Xian Li, Xi Victoria Lin, et al. Opt: Open pre-trained transformer
 671 language models. *arXiv preprint arXiv:2205.01068*, 2022.

672 Zaibin Zhang, Shiyu Tang, Yuanhang Zhang, Talas Fu, Yifan Wang, Yang Liu, Dong Wang, Jing
 673 Shao, Lijun Wang, and Huchuan Lu. Ad-h: Autonomous driving with hierarchical agents. *arXiv
 674 preprint arXiv:2406.03474*, 2024.
 675

676 Lianmin Zheng, Wei-Lin Chiang, Ying Sheng, Siyuan Zhuang, Zhanghao Wu, Yonghao Zhuang,
 677 Zi Lin, Zhuohan Li, Dacheng Li, Eric. P Xing, Hao Zhang, Joseph E. Gonzalez, and Ion Stoica.
 678 Judging llm-as-a-judge with mt-bench and chatbot arena, 2023.

679 Yinan Zheng, Ruiming Liang, Kexin Zheng, Jinliang Zheng, Liyuan Mao, Jianxiong Li, Weihao
 680 Gu, Rui Ai, Shengbo Eben Li, Xianyuan Zhan, et al. Diffusion-based planning for autonomous
 681 driving with flexible guidance. *arXiv preprint arXiv:2501.15564*, 2025.

682 Deyao Zhu, Jun Chen, Xiaoqian Shen, Xiang Li, and Mohamed Elhoseiny. Minigpt-4: En-
 683 hancing vision-language understanding with advanced large language models. *arXiv preprint
 684 arXiv:2304.10592*, 2023.
 685

686

687

688

689

690

691

692

693

694

695

696

697

698

699

700

701